Shubnikov–de Haas oscillations reaching the quantum limit in two-dimensional electron systems at $SrTiO_3$ (111) interfaces

Ziqiao Wang [1,*,†] Autumn Heltman [1,*] Shalini Kumari,[1] Lunhui Hu [1] Zhu Lin,[1] Rojin Taheri,[2] Leixin Miao,[2] Nasim Alem,[2] Lin Jiao [3] Shalinee Chikara [3] Alexey Suslov [3] John Singleton [4] Fedor Balakirev [4] Chaoxing Liu,[1] and Qi Li [1,‡]

[1]*Department of Physics, The Pennsylvania State University, University Park, Pennsylvania 16802, USA*
[2]*Department of Materials Science and Engineering, The Pennsylvania State University, University Park, Pennsylvania 16802, USA*
[3]*National High Magnetic Field Laboratory, Tallahassee, Florida 32310, USA*
[4]*National High Magnetic Field Laboratory, Los Alamos National Laboratory, Los Alamos, New Mexico 87545, USA*

(Received 20 October 2021; revised 3 May 2022; accepted 7 July 2025; published 21 July 2025)

Transition metal oxides in the (111) orientation have been predicted to harbor topological phases and unconventional quantum states because of their hexagonal crystal symmetry and strong interactions between charge, spin, and orbital degrees of freedom. We report Shubnikov–de Haas oscillations into the quantum limit at magnetic fields up to 35 T in high-mobility ($>20\,000$ $cm^2\,V^{-1}\,s^{-1}$) two-dimensional electron liquids at (111)-oriented $SrTiO_3$ interfaces with controllable carrier densities. Spin splitting is observed at low Landau levels, which is attributed to the interplay between the Zeeman splitting and Rashba spin-orbit coupling according to our theoretical modeling, yielding Landé factor $g = 0.29$ and Rashba coefficient $\alpha = 0.6$ meV nm. At high magnetic field after the system reaches the lowest Landau level, the temperature dependence of the resistance shows a metallic to insulating state transition with the magnetoresistance changing significantly from a primarily quadratic to a large linear field dependence.

DOI: 10.1103/why6-1fl8

I. INTRODUCTION

Transition metal oxides in the (111) orientation have recently attracted special interest [1–14] owing to a combination of hexagonal crystal symmetry, strongly correlated *d*-orbital electrons, and large spin-orbit coupling (SOC) effect [1–6]. With strong electron-electron interaction, Wigner crystal [1], topological Mott insulator [2–4], spin liquid [4–6] and unique magnetic ground states [6] have been predicted in such systems. Specifically, in $SrTiO_3$ (111), the top two TiO_6 layers form a buckled honeycomb lattice which is similar to the structure of graphene and bilayer transition metal dichalcogenides [15,16]. Dirac bands and charge-ordered insulating phases have been predicted by density functional theory calculations based on the honeycomb lattice with on-site Coulomb interaction [2], but they have yet to be realized experimentally.

The discovery of a two-dimensional (2D) electron system at the interface between two band insulators, $SrTiO_3$ and $LaAlO_3$, has opened up new and uncharted territory for condensed matter physics and materials science [17,18]. Rich quantum properties are revealed in $SrTiO_3$ (001)-based interfaces and surfaces [19–38], including the quantum Hall effect [24,25], coexistence of superconductivity and ferromagnetism [26–31], and a large Rashba SOC [33,34]. The $SrTiO_3$ (001) interface has also shown strong potential for spintronics applications because of the unprecedented spin-charge conversion efficiency [34]. Compared to the (001)-oriented interfaces, $SrTiO_3$ (111)-based 2D electron systems have been scarcely studied due to the difficulty in fabricating samples with high mobility. However, based on results thus far reported, the (111) systems have already shown distinct electronic properties in comparison with those of the (001) orientation [7–12]. The differences are attributed to the different symmetry [8–11] and strong electronic correlations [11,12]. For instance, our previous results on $SrTiO_3$ (111) surface electron systems have demonstrated that its in-plane anisotropic magnetoresistance (MR) has a sixfold symmetry [10], in contrast to the fourfold symmetry in the (001) orientation, reflecting the difference in orbital symmetry of the band structures. Shubnikov–de Haas (SdH) oscillations provide a powerful measurement tool to probe the electronic states at the Fermi surface and have been widely applied to the $SrTiO_3$ (001) system [35–38]. However, due to low mobility or three-dimensional nature of the previous samples, the SdH effect has been rarely reported for $SrTiO_3$ (111) [11].

II. METHOD

In the exploration of the intriguing quantum properties of (111) systems, we have developed a fabrication process using dual layer amorphous semiconductors to create a 2D electron liquid at (111)-oriented $SrTiO_3$ interfaces with high mobility ($>20\,000$ $cm^2\,V^{-1}\,s^{-1}$) and controllable carrier density. 2D electron systems were formed at interfaces between $SrTiO_3$

*These authors contributed equally to this work.
†Contact author: wangziqiao@quantumsc.cn
‡Contact author: qil1@psu.edu

TABLE I. Parameters for sample A, B, C, and D. R_s is the sheet resistance, n_{Hall} is determined by $n_{\mathrm{Hall}} = 1/eR_{\mathrm{H}}$ where R_{H} is the Hall coefficient defined by the slope of $R_{xy}(B)$ at low fields, n_{SdH} is calculated from the SdH oscillation frequency B_f by $n_{\mathrm{SdH}} = (2e/h)B_f$, and B_q is obtained directly from the experimental data as the last dip of the SdH oscillations.

Sample	R_s at ~0.3 K (Ohm)	n_{Hall} at ~0.3 K ($\times 10^{13}$ cm^{-2})	μ_{Hall} at ~0.3 K (cm^2 V^{-1} s^{-1})	n_{SdH} at ~0.3 K ($\times 10^{12}$ cm^{-2})	B_f (T)	B_q (T)
A	11.6	3.52	15 200	1.20	24.4	19.9
B	17.1	2.59	14 100	0.98	20.2	16.5
C	18.4	2.39	14 300	1.08	22.3	18.0
D	70.0	1.24	7200	0.68	14.7	12.6

(111) single crystals and SiO_2 thin films. For the purposes of this study, 60-nm-thick SiO_2 films were deposited by RF sputtering at room temperature. The thickness does not significantly affect the properties of the 2D electron systems unless it is very thin (<5 nm) [39]. A thin HfO_2 buffer layer (3–13 nm) was constructed at the interface before the SiO_2 deposition to control the carrier density and dimensionality [40]. HfO_2 films were fabricated by atomic layer deposition (ALD) at 110 °C using tetrakis (dimethylamido) hafnium [$Hf(NMe_2)_4$] as the metal precursor and water as the oxygen source [41,42], and subsequently annealed in oxygen at 110 °C for several hours. Electrical transport measurements showed that the ALD deposited HfO_2 films were very insulating.

X-ray diffraction (XRD) measurements have been conducted for $SrTiO_3$ (111)/HfO_2/SiO_2 interface samples [Fig. S1(a) [43]]. Besides the single-crystal $SrTiO_3$ (111) peak, no diffraction peaks were observed from either SiO_2 or HfO_2 layers, indicating that both SiO_2 and HfO_2 layers are in their amorphous phases. This is consistent with the results for thicker HfO_2 and SiO_2 films deposited at low substrate temperatures that they are both in amorphous phases. A high-resolution cross-sectional transmission electron microscopy (TEM) image of a typical sample with 3 nm HfO_2 and 60 nm SiO_2 is shown in Fig. S1(b) [43]. The ALD-deposited HfO_2 film is rather uniform in thickness. The sharp interfaces are further confirmed by the element mappings using energy-dispersive spectroscopy (EDS) [Figs. S1(c) and S1(d); see the Supplemental Material [43] and Refs. [44,45] therein]. The TEM images confirm that the $SrTiO_3$ (111) single crystal has a perfect crystal structure, while both SiO_2 and HfO_2 layers are amorphous.

The device was fabricated using the following procedure. After the first photolithography step, a 5 nm Ti /50 nm Au film was deposited as the contact leads on the surface of the single crystal after a light ion milling. A Hall bar of size 20 μm × 100 μm was patterned, followed by the HfO_2 and SiO_2 deposition. The longitudinal resistance R_{xx} and Hall resistance R_{xy} were measured using standard four-probe *ac* techniques. The samples reported in this paper have Hall carrier densities in the low 10^{13} cm^{-2} range with relatively small contact resistances (samples A, B, C, and D have Hall carrier densities of 3.52, 2.59, 2.39, and 1.24 $\times 10^{13}$ cm^{-2}, respectively, shown in Table I). Transport measurements at National High Magnetic Field Laboratory (NHMFL) were carried out in a He-3 cryostat with DC fields of up to 35 T and a base temperature of 300 mK. A rotation probe was used to measure the SdH oscillations at different angles, which was calibrated using the Hall resistance of the sample.

III. EXPERIMENTAL RESULTS AND DISCUSSION

A. Magnetoresistance behavior at $SrTiO_3$ (111) interface

The sheet resistance $R_s(T) = \frac{R_{xx}(T)}{L/W}$ (L is the length and W is the width of the Hall bar) of sample A is presented in the inset of Fig. 1. R_s decreases with decreasing temperatures, with a residual resistance ratio $\frac{R_s(290\ \mathrm{K})}{R_s(0.3\ \mathrm{K})} = 1563$, indicating the highly metallic nature of the 2D electron system. Magnetoresistance measurements were conducted in high magnetic fields of up to 35 T and at low temperatures down to 300 mK (performed at NHMFL in Tallahassee, Florida). Figure 1 displays R_s for sample A with the magnetic field applied perpendicular to the interface. The corresponding MR is defined as $MR(B) = \frac{[R_s(B) - R_s(0\ T)]}{R_s(0\ T)} \times 100\%$. Clear resistance oscillations are observed from lower fields to around 20 T. Above this field, the oscillations disappear and the MR changes behavior, resulting a sharp rise in resistance. With their lower carrier densities, samples B, C, and D also exhibit oscillations and a larger increase of MR at higher fields [Fig. S2(a) [43]]. The critical magnetic field at which the last oscillation occurs decreases with reducing carrier density. The effect of

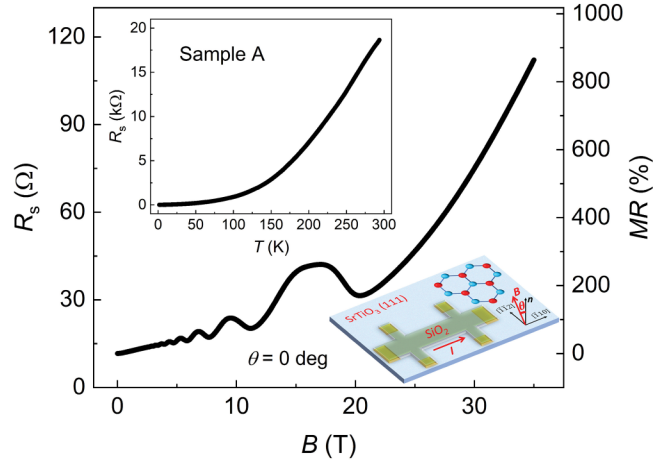

FIG. 1. Sheet resistance R_s versus magnetic field at high magnetic field up to 35 T and 320 mK in sample A. Upper inset: R_s versus temperature. Lower inset: A schematic drawing for transport measurements. The top two layers of Ti atoms at (111) surface of $SrTiO_3$ forms a honeycomb lattice when projected to the (111) plane.

back-gate tuning on the SdH oscillations has also been studied in sample C (Table S1 [43]). However, despite apparent changes in the carrier density indicated by Hall measurements, the effect of gate voltage on SdH oscillations is relatively small compared to that caused by the variations in the initial carrier density (Fig. S3 [43]). We therefore focus our analysis on samples with different virgin carrier density.

B. Shubnikov–de Haas oscillations reaching the lowest Landau level

To further analyze the oscillations, a polynomial background $R_0(B)$ is subtracted (Fig. S4 [43]) and $\frac{\Delta R_s}{R_0} = \frac{R_s - R_0}{R_0}$ is plotted as a function of $1/B$. The result for sample A is shown in Fig. 2(a). The data show pronounced oscillations starting at low magnetic field around 2 T, reflecting high carrier mobility. The oscillations are periodic in $1/B$, strongly suggesting that they are due to the SdH effect. Generally, the SdH oscillations in 2D electron systems follow the Lifshitz-Kosevich (L-K) formula $\Delta R_s/R_0 \propto R_T R_D \cos[2\pi(\frac{B_f}{B} + \gamma)]$ [35–37,46–48]. Here $R_0(B)$ is the nonoscillatory background resistance, $R_T = \beta T/\sinh(\beta T)$ is the thermal damping term, $R_D = \exp(-\beta T_D)$ is the Dingle damping factor; $\beta T = 2\pi^2 k_B T m^*/\hbar e B$, $T_D = \hbar/2\pi k_B \tau_q$ is the Dingle temperature, m^* is the effective mass, τ_q is the quantum scattering time, and B_f is the SdH oscillation frequency. The phase factor $2\pi\gamma$ comes from Berry's geometrical phase [49–51]. We observe that $\Delta R_s/R_0$ follows a single-band L-K formula for all oscillations except the last oscillation, which has a slightly larger oscillation amplitude than expected. This may be due to two reasons: (1) the L-K formula is strictly valid only for small values of $\Delta R_s/R_0$ [52], and (2) there is a sharp rise of the MR in the high field range which may affect the chosen background. The best fit to the L-K formula yields $\tau_q = 2$ ps, which is shorter than the transport scattering time $\tau_t = \frac{m^*\mu}{e} =$ 12 ps, commonly observed in electron gas systems [43]. A phase factor of $\gamma = 0.37$ is obtained from the L-K fitting, corresponding to a nonzero Berry phase of 0.27π. This is likely originated from the degeneracy of electron states and SOC in the system [7,49–51].

A Landau fan diagram is plotted in Fig. 2(b), where the integer Landau level index (n) is assigned to the nth oscillation dip in Fig. 2(a). As indicated in the figure, the Landau level $n = 1$ has been reached at the last oscillation dip, beyond which only the lowest Landau level is occupied and all higher Landau levels are empty. This is commonly referred to as the quantum limit [53]. No more resistance oscillations are observed at higher fields. The dip and peak positions in the inversed magnetic field have a linear relationship with n, and the slope of the linear fitting gives $B_f = 24.4 \pm 0.1$ T. Furthermore, fast Fourier transformation (FFT) analysis of the oscillations presented in Fig. 2(a) is characterized by a sharp single peak [the inset of Fig. 2(b)], indicating once again the single band feature of the oscillation. The FFT peak position is at $B_f = 24.4 \pm 0.4$ T, which is consistent with the frequency given by the linear fitting (24.4 ± 0.1 T) and the L-K fitting (24.3 ± 0.1 T).

The SdH oscillations are studied in four samples with different initial carrier densities (Table I and Fig. S2 [43]). All the samples exhibit clear SdH oscillations reaching the

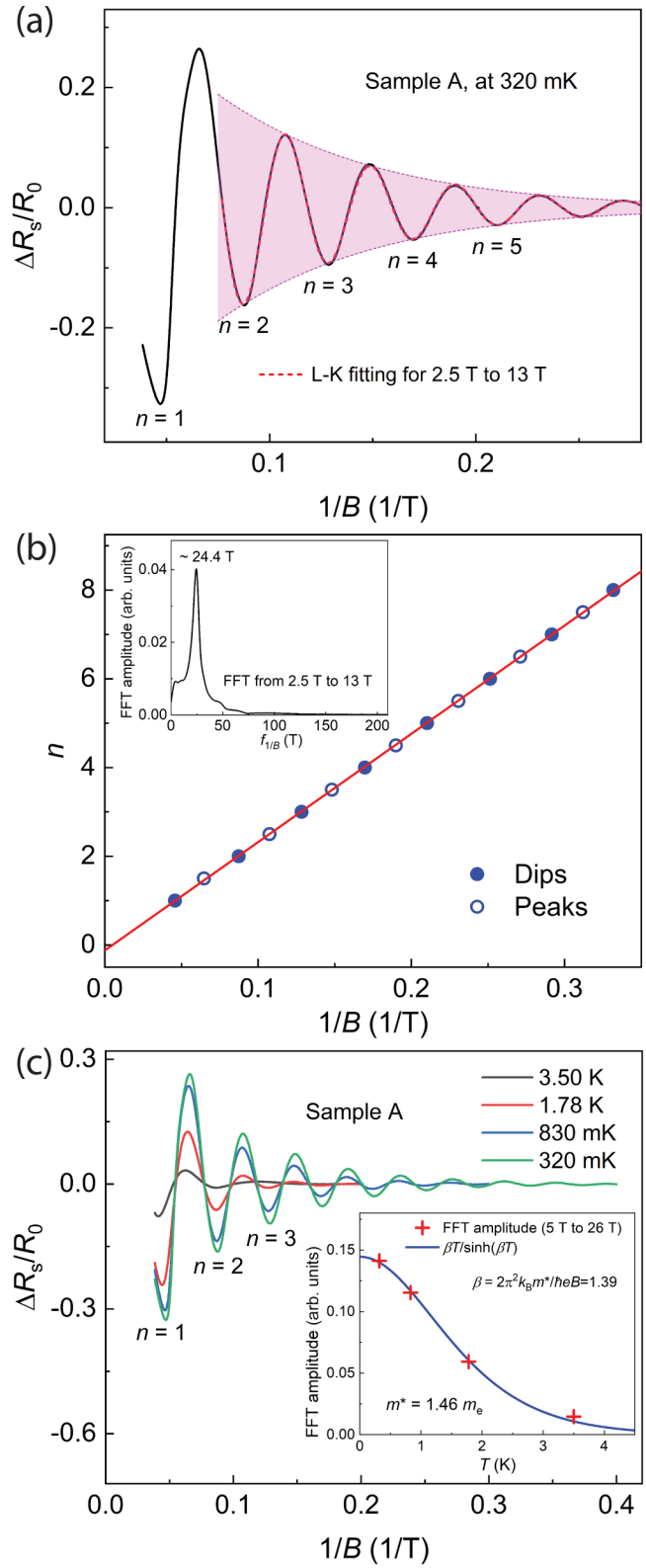

FIG. 2. (a) $\Delta R_s/R_0$ has a periodicity in $1/B$ indicating the SdH oscillations. Oscillations for Landau level $n \geqslant 2$ follows the trendline given by L-K formula. (b) Landau fan diagram. The integer Landau level index (n) is assigned to the nth oscillation dip. Inset: Fast Fourier transformation of $\Delta R_s/R_0$ from 2.5 to 13 T. (c) $\Delta R_s/R_0$ plotted as a function of $1/B$ at temperatures of 0.32 K, 0.83 K, 1.78 K, and 3.50 K, respectively. Inset: Temperature dependence of the SdH FFT amplitude (5–26 T) gives the effective mass $m^* = 1.46 \pm 0.05\, m_e$.

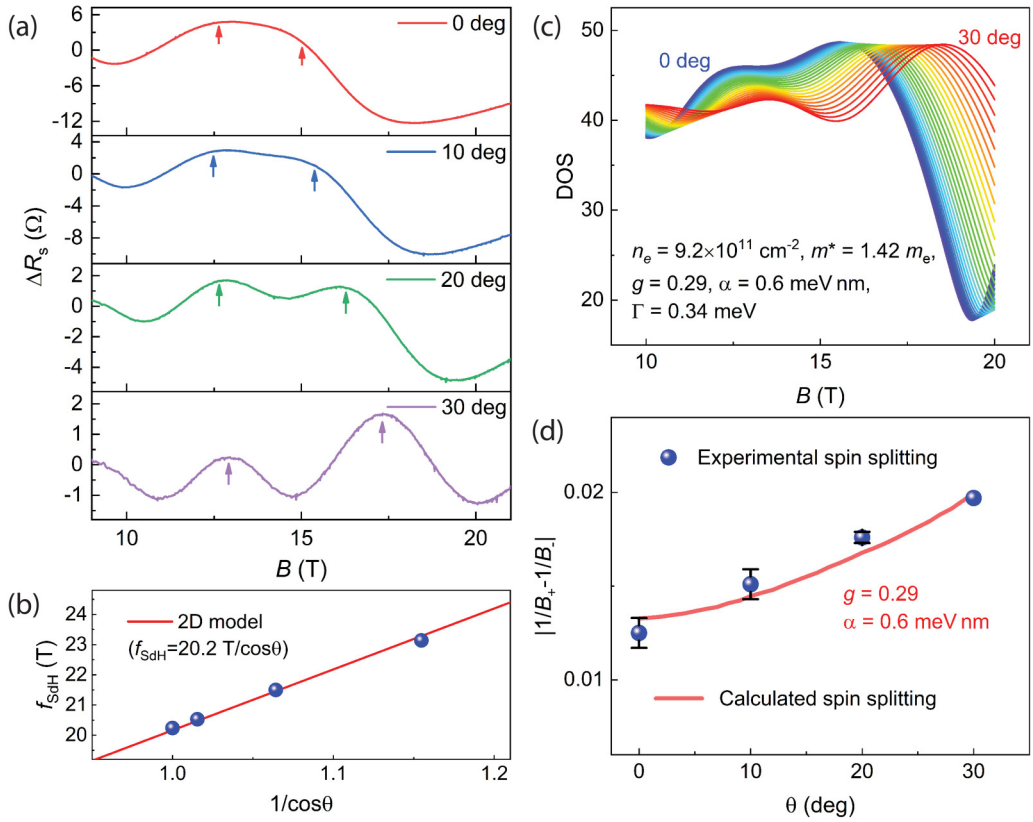

FIG. 3. (a) Spin splitting for last oscillation peak in sample B at several magnetic field angles. (b) The SdH oscillation frequency scales linearly with $^{1}/_{\cos\theta}$, indicating a 2D nature of the electron system. (c) DOS considering both Rashba SOC and Zeeman splitting for different magnetic field angles, which can qualitatively reproduce experimental observation. (d) Comparison of experimental and calculated split $|\frac{1}{B_+} - \frac{1}{B_-}|$.

lowest Landau level as represented by the last resistance dip at the quantum limit field B_q. Above B_q, the resistance depends linearly on magnetic field. Further support for this assertion comes from plotting $-\mathrm{d}^2R_s/\mathrm{d}B^2$, which reaches the last dip at B_q and tends to zero at higher fields [Fig. S5(a) [43]]. From samples A to D sorted by decreasing carrier densities, B_q changes from 19.9 T to 12.6 T, respectively. The intercepts in the Landau fan diagram are almost identical for all samples [Fig. S5(b) [43]]. This consistency of the nonzero intercept for different samples demonstrates again the nonzero Berry phase in the electron system at $SrTiO_3$ (111) interface. Owing to the nonzero Berry phase, B_q is slightly lower than the SdH oscillation frequency B_f. Both B_f and B_q shift to lower fields with lower carrier density [Fig. S5(c) [43]]. This is consistent with the Onsager relation since the cross-sectional area of the 2D Fermi contour becomes smaller with lower carrier density.

Hall resistance at or above 4 K shows a linear field dependence [Fig. S6(a) [43]]. Hall plateaus (Hall resistance slope reductions) appear in Hall resistance measured at lower temperatures, suggestive of the quantum Hall-like effect [Fig. S6(b) [43]]. We notice that the carrier density determined from the SdH oscillation frequency is lower than that obtained from Hall resistance. The discrepancy has also been widely reported in $SrTiO_3$ (001) systems and attributed to the multiband character and band degeneracy [18,25,36,38]. Considering the linear Hall effect and a single SdH oscillation frequency, the discrepancy in the $SrTiO_3$ (111) system is more likely due to the band degeneracy rather than the multiband character. ARPES results and band calculations on the $SrTiO_3$ (111) surface have shown three equivalent Fermi surface ellipses, indicating a valley degeneracy of three [8,9]. Additionally, the band degeneracy may also originate from multiple Ti subbands. It was proposed that multiple Ti subbands with similar mobility and effective mass in oxide interface quantum well could give rise to combined SdH oscillations [25].

C. Angular dependence of spin splitting

We observe extra features in the region of low Landau level quantum numbers. As noted in Fig. 1, the last oscillation peak has a wider top, resembling a superposition of two peaks rather than a single oscillation peak. This feature is reminiscent of spin splitting at high magnetic fields. The peak splitting is seen more clearly when the field is tilted from the out-of-plane orientation. We show in Fig. 3(a) the angular dependence of the last oscillation peak in sample B. The angular behavior of sample A is similar (Fig. S7 [43]). At 20° and 30° angles, the last peak clearly splits into two peaks. The SdH oscillation frequency scales linearly with $^{1}/_{\cos\theta}$, suggesting a 2D nature of the electron system [Fig. 3(b) and Fig. S8 [43]]. Meanwhile the oscillation amplitude gradually decreases with increasing angles (from ~10 ohm at $\theta = 0°$ to ~1 ohm at $\theta = 30°$). The SdH oscillation is very weak and not extractable under in-plane magnetic field (Fig. S9 [43]). To

determine the peak splitting value for the perpendicular field direction, we fitted the last peak with the superposition of two Lorentz peaks with the splitting $|1/B_+ - 1/B_-| = 0.013\ \mathrm{T}^{-1}$ for sample B (see Fig. S10 [43] and supplemental discussion). The split increases with increasing angle as shown in Fig. 3(d). At 30°, the splitting increases to $0.02\,\mathrm{T}^{-1}$. The shallow dip between the two spin-split peaks corresponds to a half-filling state for $n = 1$ state where the $n = 0$ state is fully occupied while only one spin state is occupied for $n = 1$ state (Fig. S11 [43]). Note that the lift of spin degeneracy at high field has also been reported at $SrTiO_3$ (001) interface, where the doubling of the SdH frequency at high field suggests a transition from spin-degenerate to spin-resolved state [25]. The spin splitting has been observed in various systems and commonly used to determine the g factor by analyzing the phase shift of the split peak [54–56].

The broken inversion symmetry at the interface gives rise to intrinsic SOC. We thus consider a single-band Hamiltonian with both Rashba SOC and Zeeman splitting,

$$H_0 = \frac{\hbar^2 k^2}{2m^*} + \alpha(\sigma_x k_y - \sigma_y k_x) - \vec{\mu}_B \cdot \vec{B}. \quad (1)$$

To explain the experimental results, we calculate the density of state $\mathrm{DOS}(B, \theta)$ based on the Landau level spectrum and the assumption of a constant carrier density [43,57]. The angular-dependent peak splitting $|\frac{1}{B_+} - \frac{1}{B_-}|$ is calculated from $\mathrm{DOS}(B, \theta)$ and compared to the experimental results [Figs. 3(c) and 3(d)]. The peak-splitting trend with increasing tilt angles can be reproduced with $g = 0.29$ and Rashba parameter $\alpha = 0.6$ meV nm (see the Supplemental Material [43] for the detailed procedure to determine the parameters). The energy scale of band splitting caused by the Rashba SOC at the Fermi surface is given by $E_{\mathrm{Rashba}} = 2\alpha\sqrt{2m^* E_F}/\hbar = 0.3$ meV.

The Rashba parameter of $\alpha = 0.6$ meV nm derived from spin splitting is close to the value reported at $LaAlO_3/SrTiO_3$ (111) interface from the fit to the weak antilocalization effect [7]. It is also comparable to the value in $SrTiO_3$ (001) systems by tight-binding calculation and second harmonic bilinear magnetoresistance measurement [33,58]. The g factor is significantly smaller than that of a free electron. Noteworthily, the small g factor does not depend on the model considering Rashba SOC; a small g factor is obtained even if we assume the spin splitting to be purely due to the Zeeman effect [43]. The deviation of g factor from 2 (either larger or smaller than 2) is expected in systems with strong SOC [59]. For instance, SOC could give rise to a small g factor in $(4d)^3$ and $(5d)^3$-based transition metal oxides [60]. Moreover, the g factor can be affected by the electric field in quantum well structures [61]; a gate tunable g factor has been experimentally demonstrated at the $LaAlO_3/SrTiO_3$ (001) interface by analyzing the magnetoresistance behavior, and a small g-factor appears at negative gate voltage [62]. The small g factor at the $SrTiO_3$ (111) interface likely originates from the atomic SOC of Ti and the hybridization of three t_{2g} bands.

D. Linear magnetoresistance with insulating behavior in the quantum limit

Achieving the lowest Landau level at relatively low field enables us to study the quantum limit transport, which, to the best of our knowledge, has never been reached in $SrTiO_3$ (111) electron systems. As seen in Fig. 1, the quantum oscillations disappear after the system reaches B_q. In field region below B_q, the MR is dominated by a quadratic dependence with the field. Above B_q, there is a sudden transition to a linear field dependence with a much larger MR. This MR transition is also accompanied by a metallic to insulating state transition. At low magnetic fields, the resistance decreases with decreasing temperature; above B_q, the resistance increases with decreasing temperature (Fig. S2 [43]). Linear MR behavior at high magnetic fields above B_q is also observed in samples B, C, and D [Fig. S2(a) [43]], and because lower carrier densities result in lower B_q in these samples, the linear MR behavior appears over a wider field range than that of sample A. The MR magnitude exceeds 1400% in sample B at 35 T. Figure 4 shows the linear MR region of samples B, C, and D at high magnetic fields. Good agreement between the linear fits and experimental data are obtained. We have also made a double-logarithmic plot of $R_s - R_0$ versus magnetic field in samples B, C, and D (Fig. S12 [43]). The best fit of the power-law fitting ($R_s - R_0 \sim B^m$, where R_0 is the intercept) to the experimental data from 23 to 35 T yields m close to 1, further confirming the linear behavior.

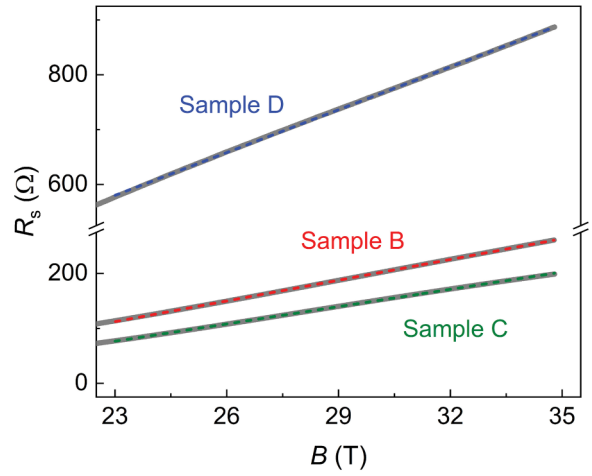

FIG. 4. Linear MR behavior at high magnetic field in the quantum limit in samples B, C, and D. Linear fitting has a good agreement with the experimental data.

We briefly discuss the possible origin of the unsaturated linear MR behavior and the metallic to insulating transition in high magnetic field. Multiple mechanisms have been developed to describe the linear MR behavior in various materials [63–71]. In our samples, the MR behavior is very distinctive from the previous reports that the MR is not linear before reaching the lowest Landau level; only once the electrons, which contribute to the SdH oscillations, are in the lowest Landau level does the MR become linear. By contrast, in Refs. [55,63,64] the MR is linear over a wide magnetic field range and it is unrelated to the system reaching the lowest Landau level. In such cases, the linear MR is frequently caused by disorder and inhomogeneities [69,70]. Since the Landau levels would be smeared in disordered systems, it is unlikely that SdH oscillations would be visible. Therefore, disorder and inhomogeneities cannot completely explain the observed linear MR in the quantum limit in our

high mobility system. In Abrikosov's quantum model [68], linear MR appears in materials with Dirac-like bands [65–67] when only the lowest Landau level is occupied. Although a Dirac-like band has been predicted at specific points in the Brillouin zone in $SrTiO_3$ (111) systems [1,2], it is believed that it is not the dominant band for the electron transport [8,9]. However, we cannot completely rule out the possibility that it becomes more pronounced when only the lowest Landau level is occupied.

Notably, the linear MR in our samples appears in a field-temperature region displaying insulating behavior [i.e., the resistance increases with decreasing temperature as shown in Figs. S2(d) and S2 (e) [43]]. Magnetic "freeze out" is proposed to explain the giant MR accompanied by insulating behavior in semiconductors such as InSb [72]. Bound states are formed as the field increases, and as a result the carriers in the conduction band become localized. However, in this model, the MR is proportional to B^3, rather than the linear field dependence seen here. On the other hand, insulating behavior could be driven by electron correlation [2–4,73–75]. It has been predicted that a charge-ordered insulating phase could appear in $SrTiO_3$ (111) heterostructures due to the combination of on-site Coulomb interaction and broken inversion symmetry [2]. The observed linear MR with insulating behavior above B_q may suggest a transition to a charge-ordered insulating phase [73]. A linear MR behavior in the quantum limit has also been reported in lightly doped single crystals of $SrTiO_3$, which is linked to magnetic-field-induced puddling of electrons [76].

IV. CONCLUSION

In summary, we have achieved a high-mobility 2D electron system with controllable carrier density at (111)-oriented $SrTiO_3$ interfaces. We observe for the first time in this system pronounced SdH oscillations into the quantum limit. Angular dependent spin splitting is observed in the low Landau level states, which is attributed to Zeeman splitting and Rashba SOC in agreement with theoretical modeling. Our model yields a small g factor, demonstrating the uniqueness of the 2D electron system at (111)-oriented interface due to the distinctive symmetry and confinement. Above the quantum limit field, the system undergoes a metallic to insulating state transition according to the temperature dependence of the resistance. Under the same conditions, the magnetoresistance changes significantly from a quadratic behavior to a linear behavior with a large MR. Our results demonstrate that the strongly correlated electron system at $SrTiO_3$ (111) interface could give rise to novel insulating states in the quantum limit.

ACKNOWLEDGMENTS

We acknowledge the helpful discussion with Jainendra Jain and Jing Wang for experimental assistance. This work was financially supported by the Department of Energy under Grants No. DE-FG02-08ER46531 for the sample fabrication and characterization and Energy Frontier Research Centers program DE-SC0021118 for the TEM measurement. Measurements conducted at the National High Magnetic Field Laboratory (NHMFL) were supported by NSF DMR-1905833. NHMFL is supported by NSF Cooperative Agreements (No. DMR-1644779 and DMR-2128556) and the state of Florida. J.S. acknowledges funding from the DoE Basic Energy Science Program "Science at 100 T." Theoretical modeling (C.L.) was supported by the Office of Naval Research (Grant No. N00014-18-1–2793).

DATA AVAILABILITY

The data that support the findings of this article are not publicly available. The data are available from the contact authors upon reasonable request.

[1] D. Xiao, W. Zhu, Y. Ran, N. Nagaosa, and S. Okamoto, Interface engineering of quantum Hall effects in digital transition metal oxide heterostructures, Nat. Commun. **2**, 596 (2011).

[2] D. Doennig, W. E. Pickett, and R. Pentcheva, Massive symmetry breaking in $LaAlO_3/SrTiO_3$ (111) quantum wells: A three-orbital strongly correlated generalization of graphene, Phys. Rev. Lett. **111**, 126804 (2013).

[3] Y. Tokura and N. Nagaosa, Orbital physics in transition-metal oxides, Science **288**, 462 (2000).

[4] D. Pesin and L. Balents, Mott physics and band topology in materials with strong spin–orbit interaction, Nat. Phys. **6**, 376 (2010).

[5] S. H. Chun, J.-W. Kim, J. Kim, H. Zheng, C. C. Stoumpos, C. D. Malliakas, J. F. Mitchell, K. Mehlawat, Y. Singh, Y. Choi, T. Gog, A. Al-Zein, M. M. Sala, M. Krisch, J. Chaloupka, G. Jackeli, G. Khaliullin, and B. J. Kim, Direct evidence for dominant bond-directional interactions in a honeycomb lattice iridate Na_2IrO_3, Nat. Phys. **11**, 462 (2015).

[6] J. G. Rau, E. K.-H. Lee, and H.-Y. Kee, Generic spin model for the honeycomb iridates beyond the Kitaev limit, Phys. Rev. Lett. **112**, 077204 (2014).

[7] E. Lesne, Y. G. Sağlam, R. Battilomo, M. T. Mercaldo, T. C. van Thiel, U. Filippozzi, C. Noce, M. Cuoco, G. A. Steele, C. Ortix, and A. D. Caviglia, Designing spin and orbital sources of Berry curvature at oxide interfaces, Nat. Mater. **22**, 576 (2023).

[8] S. M. Walker, A. de la Torre, F. Y. Bruno, A. Tamai, T. K. Kim, M. Hoesch, M. Shi, M. S. Bahramy, P. D. C. King, and F. Baumberger, Control of a two-dimensional electron gas on $SrTiO_3$ (111) by atomic oxygen, Phys. Rev. Lett. **113**, 177601 (2014).

[9] T. C. Rödel, C. Bareille, F. Fortuna, C. Baumier, F. Bertran, P. Le Fèvre, M. Gabay, O. H. Cubelos, M. J. Rozenberg, T. Maroutian, P. Lecoeur, and A. F. Santander-Syro, Orientational tuning of the Fermi sea of confined electrons at the $SrTiO_3$ (110) and (111) surfaces, Phys. Rev. Appl. **1**, 051002(R) (2014).

[10] L. Miao, R. Du, Y. Yin, and Q. Li, Anisotropic magnetotransport properties of electron gases at $SrTiO_3$ (111) and (110) surfaces, Appl. Phys. Lett. **109**, 261604 (2016).

[11] U. Khanna, P. K. Rout, M. Mograbi, G. Tuvia, I. Leermakers, U. Zeitler, Y. Dagan, and M. Goldstein, Symmetry and correla-

tion effects on band structure explain the anomalous transport properties of (111) $LaAlO_3/SrTiO_3$, Phys. Rev. Lett. **123**, 036805 (2019).

[12] A. M. R. V. L. Monteiro, M. Vivek, D. J. Groenendijk, P. Bruneel, I. Leermakers, U. Zeitler, M. Gabay, and A. D. Caviglia, Band inversion driven by electronic correlations at the (111) $LaAlO_3/SrTiO_3$ interface, Phys. Rev. B **99**, 201102(R) (2019).

[13] P. K. Rout, E. Maniv, and Y. Dagan, Link between the superconducting dome and spin-orbit interaction in the (111) $LaAlO_3/SrTiO_3$ interface, Phys. Rev. Lett. **119**, 237002 (2017).

[14] N. Boudjada, G. Wachtel, and A. Paramekanti, Magnetic and nematic orders of the two-dimensional electron gas at oxide (111) surfaces and interfaces, Phys. Rev. Lett. **120**, 086802 (2018).

[15] E. C. Regan, D. Wang, C. Jin, M. I. B. Utama, B. Gao, X. Wei, S. Zhao, W. Zhao, Z. Zhang, K. Yumigeta, M. Blei, J. D. Carlström, K. Watanabe, T. Taniguchi, S. Tongay, M. Crommie, A. Zettl, and F. Wang, Mott and generalized Wigner crystal states in WSe_2/WS_2 moiré superlattices, Nature (London) **579**, 359 (2020).

[16] T. Li, S. Jiang, L. Li, Y. Zhang, K. Kang, J. Zhu, K. Watanabe, T. Taniguchi, D. Chowdhury, L. Fu, J. Shan, and K. F. Mak, Continuous Mott transition in semiconductor moiré superlattices, Nature (London) **597**, 350 (2021).

[17] A. Ohtomo and H. Y. Hwang, A high-mobility electron gas at the $LaAlO_3/SrTiO_3$ heterointerface, Nature (London) **427**, 423 (2004).

[18] Y.-Y. Pai, A. Tylan-Tyler, P. Irwin, and J. Levy, Physics of $SrTiO_3$-based heterostructures and nanostructures: A review, Rep. Prog. Phys. **81**, 036503 (2018).

[19] M. Basletic, J.-L. Maurice, C. Carrétéro, G. Herranz, O. Copie, M. Bibes, É. Jacquet, K. Bouzehouane, S. Fusil, and A. Barthélémy, Mapping the spatial distribution of charge carriers in $LaAlO_3/SrTiO_3$ heterostructures, Nat. Mater. **7**, 621 (2008).

[20] B. Huang, Y. Chiu, P. Huang, W. Wang, V. T. Tra, J. Yang, Q. He, J. Lin, C. Chang, and Y. Chu, Mapping band alignment across complex oxide heterointerfaces, Phys. Rev. Lett. **109**, 246807 (2012).

[21] Z. Q. Liu, C. J. Li, W. M. Lü, X. H. Huang, Z. Huang, S. W. Zeng, X. P. Qiu, L. S. Huang, A. Annadi, J. S. Chen, J. M. D. Coey, T. Venkatesan, and Ariando, Origin of the two-dimensional electron gas at $LaAlO_3/SrTiO_3$ interfaces: The role of oxygen vacancies and electronic reconstruction, Phys. Rev. X **3**, 021010 (2013).

[22] H. W. Jang, D. A. Felker, C. W. Bark, Y. Wang, M. K. Niranjan, C. T. Nelson, Y. Zhang, D. Su, C. M. Folkman, S. H. Baek, S. Lee, K. Janicka, Y. Zhu, X. Q. Pan, D. D. Fong, E. Y. Tsymbal, M. S. Rzchowski, and C. B. Eom, Metallic and insulating oxide interfaces controlled by electronic correlations, Science **331**, 886 (2011).

[23] M. Lee, J. R. Williams, S. Zhang, C. D. Frisbie, and D. Goldhaber-Gordon, Electrolyte gate-controlled Kondo effect in $SrTiO_3$, Phys. Rev. Lett. **107**, 256601 (2011).

[24] Y. Matsubara, K. S. Takahashi, M. S. Bahramy, Y. Kozuka, D. Maryenko, J. Falson, A. Tsukazaki, Y. Tokura, and M. Kawasaki, Observation of the quantum Hall effect in δ-doped $SrTiO_3$, Nat. Commun. **7**, 11631 (2011).

[25] F. Trier, G. E. D. K. Prawiroatmodjo, Z. Zhong, D. V. Christensen, M. von Soosten, A. Bhowmik, J. M. G. Lastra, Y. Chen, T. S. Jespersen, and N. Pryds, Quantization of Hall resistance at the metallic interface between an oxide insulator and $SrTiO_3$, Phys. Rev. Lett. **117**, 096804 (2016).

[26] N. Reyren, S. Thiel, A. D. Caviglia, L. F. Kourkoutis, G. Hammerl, C. Richter, C. W. Schneider, T. Kopp, A.-S. Rüetschi, D. Jaccard, M. Gabay, D. A. Muller, J.-M. Triscone, and J. Mannhart, Superconducting interfaces between insulating oxides, Science **317**, 1196 (2007).

[27] A. D. Caviglia, S. Gariglio, N. Reyren, D. Jaccard, T. Schneider, M. Gabay, S. Thiel, G. Hammerl, J. Mannhart, and J.-M. Triscone, Electric field control of the $LaAlO_3/SrTiO_3$ interface ground state, Nature (London) **456**, 624 (2008).

[28] A. Brinkman, M. Huijben, M. van Zalk, J. Huijben, U. Zeitler, J. C. Maan, W. G. van der Wiel, G. Rijnders, D. H. A. Blank, and H. Hilgenkamp, Magnetic effects at the interface between non-magnetic oxides, Nat. Mater. **6**, 493 (2007).

[29] D. A. Dikin, M. Mehta, C. W. Bark, C. M. Folkman, C. B. Eom, and V. Chandrasekhar, Coexistence of superconductivity and ferromagnetism in two dimensions, Phys. Rev. Lett. **107**, 056802 (2011).

[30] J. A. Bert, B. Kalisky, C. Bell, M. Kim, Y. Hikita, H. Y. Hwang, and K. A. Moler, Direct imaging of the coexistence of ferromagnetism and superconductivity at the $LaAlO_3/SrTiO_3$ interface, Nat. Phys. **7**, 767 (2011).

[31] L. Li, C. Richter, J. Mannhart, and R. C. Ashoori, Coexistence of magnetic order and two-dimensional superconductivity at $LaAlO_3/SrTiO_3$ interfaces, Nat. Phys. **7**, 762 (2011).

[32] A. Joshua, S. Pecker, J. Ruhman, E. Altman, and S. Ilani, A universal critical density underlying the physics of electrons at the $LaAlO_3/SrTiO_3$ interface, Nat. Commun. **3**, 1129 (2012).

[33] P. D. C. King, S. M. Walker, A. Tamai, A. de la Torre, T. Eknapakul, P. Buaphet, S.-K. Mo, W. Meevasana, M. S. Bahramy, and F. Baumberger, Quasiparticle dynamics and spin-orbital texture of the $SrTiO_3$ two-dimensional electron gas, Nat. Commun. **5**, 3414 (2014).

[34] E. Lesne, Y. Fu, S. Oyarzun, J. C. Rojas-Sanchez, D. C. Vaz, H. Naganuma, G. Sicoli, J. P. Attane, M. Jamet, E. Jacquet, J. M. George, A. Barthélémy, H. Jaffres, A. Fert, M. Bibes, and L. Vila, Highly efficient and tunable spin-to-charge conversion through Rashba coupling at oxide interfaces, Nat. Mater. **15**, 1261 (2016).

[35] Y. Kozuka, M. Kim, C. Bell, B. G. Kim, Y. Hikita, and H. Y. Hwang, Two-dimensional normal-state quantum oscillations in a superconducting heterostructure, Nature (London) **462**, 487 (2009).

[36] M. B. Shalom, A. Ron, A. Palevski, and Y. Dagan, Shubnikov–de Haas oscillations in $SrTiO_3/LaAlO_3$ interface, Phys. Rev. Lett. **105**, 206401 (2010).

[37] A. D. Caviglia, S. Gariglio, C. Cancellieri, B. Sacepe, A. Fete, N. Reyren, M. Gabay, A. F. Morpurgo, and J. M. Triscone, Two-dimensional quantum oscillations of the conductance at interfaces, Phys. Rev. Lett. **105**, 236802 (2010).

[38] Y. Xie, C. Bell, M. Kim, H. Inoue, Y. Hikita, and H. Y. Hwang, Quantum longitudinal and Hall transport at the $LaAlO_3/SrTiO_3$ interface at low electron densities, Solid State Commun. **197**, 25 (2014).

[39] A. Heltman, Z. Lin, Z. Wang, S. Kumari, and Q. Li (unpublished).

[40] L. Miao, J. Wang, R. Du, B. Bedford, N. Huber, K. Wang, J.-H. Park, D. Graf, and Q. Li, Dimensionality control of a novel electron gas based on $KTaO_3$ (001) interface using a spacing layer (unpublished).

[41] A. B. Mukhopadhyay, C. B. Musgrave, and J. Fdez. Sanz, Atomic layer deposition of hafnium oxide from hafnium chloride and water, J. Am. Chem. Soc. **130**, 11996 (2008).

[42] M. Kotilainen, R. Krumpolec, D. Franta, P. Souček, T. Homola, D. C. Cameron, and P. Vuoristo, Hafnium oxide thin films as a barrier against copper diffusion in solar absorbers, Solar Energy Materials Solar Cells **166**, 140 (2017).

[43] See Supplemental Material at http://link.aps.org/supplemental/10.1103/why6-1fl8 for supplemental data and discussions.

[44] R. Tan, Y. Azuma, and I. Kojima, Comparative study of the interfacial characteristics of sputter-deposited HfO_2 on native SiO_2/Si (100) using *in situ* XPS, AES and GIXR. Surf. Interface Anal. **38**, 784 (2006).

[45] X. Li, T. Yajima, T. Nishimura, K. Nagashio, and A. Toriumi, HfO_2-assisted SiO_2 reduction in HfO_2/SiO_2/Si stacks, Thin Solid Films **557**, 272 (2014).

[46] I. M. Lifshitz and A. M. Kosevich, Theory of magnetic susceptibility in metals at low temperature, Sov. Phys. JETP **2**, 636 (1956).

[47] D. Shoenberg, *Magnetic Oscillations in Metals* (Cambridge University Press, Cambridge, 1984).

[48] P. T. Coleridge, Small-angle scattering in two-dimensional electron gases, Phys. Rev. B **44**, 3793 (1991).

[49] M. V. Berry, Quantal phase factors accompanying adiabatic changes, Proc. R. Soc. London A **392**, 45 (1984).

[50] G. P. Mikitik and Y. V. Sharlai, Manifestation of Berry's phase in metal physics, Phys. Rev. Lett. **82**, 2147 (1999).

[51] M. J. Veit, R. Arras, B. J. Ramshaw, R. Pentcheva, and Y. Suzuki, Nonzero Berry phase in quantum oscillations from giant Rashba-type spin splitting in $LaTiO_3/SrTiO_3$ heterostructures, Nat. Commun. **9**, 1458 (2018).

[52] J. Singleton, Cyclotron resonance, in *Encyclopedia of Condensed Matter Physics*, edited by F. Bassani, G. Liedl, P. Wyder (Elsevier, Amsterdam, 2005), pp. 343–355.

[53] E. N. Adams and T. D. Holstein, Energy bands in the presence of an external force field—II: Anomalous velocities, J. Phys. Chem. Solids **10**, 254 (1959).

[54] Y. Liu, X. Yuan, C. Zhang, Z. Jin, A. Narayan, C. Luo, Z. Chen, L. Yang, J. Zou, X. Wu, S. Sanvito, Z. Xia, L. Li, Z. Wang, and F. Xiu, Zeeman splitting and dynamical mass generation in Dirac semimetal $ZrTe_5$, Nat. Commun. **7**, 12516 (2016).

[55] A. Narayanan, M. D. Watson, S. F. Blake, N. Bruyant, L. Drigo, Y. L. Chen, D. Prabhakaran, B. Yan, C. Felser, T. Kong, P. C. Canfield, and A. I. Coldea, Linear magnetoresistance caused by mobility fluctuations in *n*-doped Cd_3As_2, Phys. Rev. Lett. **114**, 117201 (2015).

[56] J. Y. Liu, J. Hu, Q. Zhang, D. Graf, H. B. Cao, S. M. A. Radmanesh, D. J. Adams, Y. L. Zhu, G. F. Cheng, X. Liu, W. A. Phelan, J. Wei, M. Jaime, F. Balakirev, D. A. Tennant, J. F. DiTusa, I. Chiorescu, L. Spinu, and Z. Q. Mao, A magnetic topological semimetal $Sr_{1-y}Mn_{1-z}Sb_2$ ($y, z < 0.1$), Nat. Mater. **16**, 905 (2017).

[57] R. Gammag and C. Villagonzalo, Quenching of the DOS beats in a two-dimensional electron gas in tilted magnetic fields, Solid State Commun. **152**, 757 (2012).

[58] D. C. Vaz, F. Trier, A. Dyrdał, A. Johansson, K. Garcia, A. Barthélémy, I. Mertig, J. Barnas, A. Fert, and M. Bibes, Determining the Rashba parameter from the bilinear magnetoresistance response in a two-dimensional electron gas, Phys. Rev. Mater. **4**, 071001(R) (2020).

[59] Z. Song, S. Sun, Y. Xu, S. Nie, H. Weng, Z. Fang, and X. Dai, First principle calculation of the effective Zeeman's couplings in topological materials, in *Memorial Volume for Shoucheng Zhang*, edited by Biao Lian, Chaoxing Liu, Eugene Demler, Steven Kivelson, and Xiaoliang Qi (World Scientific, Singapore, 2021), pp. 263–281.

[60] H. Matsuura and K. Miyake, Effect of spin-orbit interaction on $(4d)^3$- and $(5d)^3$-based transition-metal oxides, J. Phys. Soc. Jpn. **82**, 073703 (2013).

[61] E. L. Ivchenkoa, A. A. Kiselev, and M. Willander, Electronic *g* factor in biased quantum wells, Solid State Commun. **102**, 375 (1997).

[62] A. D. Caviglia, M. Gabay, S. Gariglio, N. Reyren, C. Cancellieri, and J.-M. Triscone, Tunable Rashba spin-orbit interaction at oxide interfaces, Phys. Rev. Lett. **104**, 126803 (2010).

[63] R. Xu, A. Husmann, T. F. Rosenbaum, M.-L. Saboungi, J. E. Enderby, and P. B. Littlewood, Large magnetoresistance in non-magnetic silver chalcogenides, Nature (London) **390**, 57 (1997).

[64] S. Mallik, G. C. Ménard, G. Saïz, I. Gilmutdinov, D. Vignolles, C. Proust, A. Gloter, N. Bergeal, M. Gabay, and M. Bibes, From low-field Sondheimer oscillations to high-field very large and linear magnetoresistance in a $SrTiO_3$-based two-dimensional electron gas, Nano Lett. **22**, 65 (2022).

[65] X. Wang, Y. Du, S. Dou, and C. Zhang, Room temperature giant and linear magnetoresistance in topological insulator Bi_2Te_3 nanosheets, Phys. Rev. Lett. **108**, 266806 (2012).

[66] Y. F. Zhao, H. W. Liu, C. L. Zhang, H. C. Wang, J. F. Wang, Z. Q. Liu, Y. Xing, H. Lu, J. Liu, Y. Wang, S. M. Brombosz, Z. L. Xiao, S. Jia, X. C. Xie, and J. Wang, Anisotropic Fermi surface and quantum limit transport in high mobility three-dimensional Dirac semimetal Cd_3As_2, Phys. Rev. X **5**, 031037 (2015).

[67] J. M. Ok, N. Mohanta, J. Zhang, S. Yoon, S. Okamoto, E. S. Choi, H. Zhou, M. Briggeman, P. Irvin, A. R. Lupini, Y.-Y. Pai, E. Skoropata, C. Sohn, H. Li, H. Miao, B. Lawrie, W. S. Choi, G. Eres, J. Levy, and H. N. Lee, Correlated oxide Dirac semimetal in the extreme quantum limit, Sci. Adv. **7**, eabf9631 (2021).

[68] I. M. Hayes, Ross D. McDonald, N. P. Breznay, T. Helm, P. J. W. Moll, M. Wartenbe, A. Shekhter, and J. G. Analytis, Scaling between magnetic field and temperature in the high-temperature superconductor $BaFe_2(As_{1-x}P_x)_2$, Nat. Phys. **12**, 916 (2016).

[69] A. A. Abrikosov, Quantum magnetoresistance, Phys. Rev. B **58**, 2788 (1998).

[70] M. M. Parish and P. B. Littlewood, Non-saturating magnetoresistance in heavily disordered semiconductors, Nature (London) **426**, 162 (2003).

[71] J. Singleton, Temperature scaling behavior of the linear magnetoresistance observed in high-temperature superconductors, Phys. Rev. Mater. **4**, 061801(R) (2020).

[72] O. Beckman, E. Hanamura, and L. J. Neuringer, Quantum limit galvanomagnetic phenomena in *n*-InSb, Phys. Rev. Lett. **18**, 773 (1967).

[73] B. Spivak, S. V. Kravchenko, S. A. Kivelson, and X. P. A. Gao, *Colloquium*: Transport in strongly correlated two-dimensional electron fluids, Rev. Mod. Phys. **82**, 1743 (2010).

[74] J. K. Jain, *Composite Fermions* (Cambridge University Press, Cambridge, 2007).

[75] J. Yoon, C. C. Li, D. Shahar, D. C. Tsui, and M. Shayegan, Wigner crystallization and metal-insulator transition of two-dimensional holes in GaAs at $B = 0$, Phys. Rev. Lett. **82**, 1744 (1999).

[76] A. Bhattacharya, B. Skinner, G. Khalsa, and A. V. Suslov, Spatially inhomogeneous electron state deep in the extreme quantum limit of strontium titanate, Nat. Commun. **7**, 12974 (2016).